



# Synthesis, structure and luminescent recognition properties of cerium(IV) coordination polymers based on pyridine-2,6-dicarboxylic acid



Lirong Yang\*, Lanzhi Wu, Huaimin Zhang, Shuang Song, Liu Liu, Mingxue Li

Henan Key Laboratory of Polyoxometalate, Institute of Molecule and Crystal Engineering, College of Chemistry and Chemical Engineering, Henan University, Jinming Street, Kaifeng 475004, PR China

## ARTICLE INFO

### Article history:

Received 3 February 2013

Received in revised form

8 May 2013

Accepted 8 May 2013

Available online 23 May 2013

### Keywords:

Coordination polymers

Synthesis

Structure

Luminescent recognition properties

Metal-organic frameworks

Hydrothermal synthesis

## ABSTRACT

3D coordination polymers of  $\{[\text{Ce}_2(\text{PDA})_3(\text{H}_2\text{O})_3] \cdot 0.25(\text{H}_2\text{O})\}_n$  and  $\{[\text{Ce}_2(\text{PDA})(\text{HPDA})(\text{H}_2\text{O})_5\text{SO}_4] \cdot 2\text{H}_2\text{O}\}_n$  (H<sub>2</sub>PDA = pyridine-2,6-dicarboxylic acid,) have been prepared under hydrothermal conditions and characterized by elemental analyses, IR spectroscopy, thermal analyses and single crystal X-ray diffraction. In the dihydrate polymer the  $\text{SO}_4^{2-}$  anions serve as bridges between 1D wavelike chains and the adjacent parallel pyridine rings are connected through  $\pi$ – $\pi$  interactions. The striking feature of the dihydrate polymer is that 1D nanosized cavities are observed, which house guest water molecules. Weak interaction exists between Ce(IV) center and S atom (Ce...S) due to the connection of chelate  $\text{SO}_4^{2-}$  anion. A magnetic study of the dihydrate polymer confirms that it presents antiferromagnetism. Thermogravimetric and differential thermogravimetric analyses reveal that both polymers are stable at high temperature. Luminescent emissions of complexes demonstrate that they display selectivities towards  $\text{Zn}^{2+}$ ,  $\text{Hg}^+$ ,  $\text{Pb}^{2+}$ ,  $\text{Mn}^{2+}$  and  $\text{Cd}^{2+}$  or  $\text{Cu}^{2+}$  ions.

© 2013 Elsevier Ltd. All rights reserved.

## 1. Introduction

The lanthanide-based metal–organic frameworks (Ln-MOFs) have attracted special attention because of their intriguing structure and tremendous potential applications in catalysis, molecular recognition, optoelectronic devices, sensors, luminescence, molecular magnetism, gas absorption and ion exchange as well as in material sciences [1–7]. A great number of Ln-MOFs have been synthesized and characterized [8–10]. Lanthanide ions possess a larger radius and higher affinity for hard donor centers and ligands with oxygen or hybrid oxygen–nitrogen atoms, particularly multicarboxylate ligands, which are in favor of the construction of Ln-MOFs [11–19]. Especially, the highly localized f electrons of lanthanide compounds allow f–f transitions, which relate to the emission behavior of lanthanide ions within a narrow wavelength range and with high quantum yields. Consequently, the Ln-MOFs are intriguing and remarkably suitable for the fabrication of optical devices and tunable luminescent sensors as well as probes for chemical species [20–30]. One feasible strategy involving the use of multicarboxylate ligands as

the organic building block, such as pyridine-2,6-dicarboxylic acid (H<sub>2</sub>PDA) and its deprotonated anions (HPDA<sup>−</sup> and PDA<sup>2−</sup> tuned under appropriate pH value) which adopt flexible, multidentate coordination sites, and therefore may potentially provide various coordination modes which are beneficial to the construction of higher-dimensional Ln-MOFs [31–37]. Following our ongoing efforts towards the synthesis and isolation of Ln-MOFs and hoping to validate whether the new Ln-MOFs can be used for luminescent probes for certain metal ions, here we design and synthesize a series of Ln-MOFs possessing functional sites for specific luminescent selectivity recognition. We report the hydrothermal synthesis, characteristics, thermal analysis and the crystal structures of the coordination polymers formed between Ce centers and H<sub>2</sub>PDA ligands. Particular attention is focused on the emission spectra of the complexes in the presence of  $\text{Pb}^{2+}$ ,  $\text{Cd}^{2+}$ ,  $\text{Hg}^+$ ,  $\text{Zn}^{2+}$ ,  $\text{Fe}^{3+}$ ,  $\text{Cu}^{2+}$  and  $\text{Mn}^{2+}$  ions and they are compared with those of the corresponding complexes.

## 2. Experimental

### 2.1. Materials and measurements

Reagents were readily available from commercial sources and were used without further purification. Elemental analysis was

\* Corresponding author.

E-mail addresses: [lirongyang@henu.edu.cn](mailto:lirongyang@henu.edu.cn), [lirongyang@163.com](mailto:lirongyang@163.com) (L. Yang).

performed with a Perkin–Elmer 240C elemental analyzer. Fourier transform infrared (FT-IR) were recorded with an AVATAR 360 FT-IR spectrometer (KBr pellets, in the region of 4000 ~ 400  $\text{cm}^{-1}$ ). The crystal structure was determined with a Bruker Smart CCD X-ray single-crystal diffractometer. Fluorescent data were collected with an F-7000 FL spectrophotometer at room temperature. Thermogravimetric (TG) and differential thermogravimetric (DTG) analyses were conducted with a Perkin–Elmer TGA7 system under flowing  $\text{N}_2$  stream (flow rate 40 mL/min) from room temperature to 1000 °C at a heating rate of 10 K/min. Magnetic susceptibility measurements were carried out by using a Quantum Design MPMS-5 magnetometer in the temperature range of 2–300 K.

## 2.2. Synthesis of the complexes **I** and **II**

### 2.2.1. Synthesis of $\{[\text{Ce}_2(\text{PDA})_3(\text{H}_2\text{O})_3] \cdot 0.25\text{H}_2\text{O}\}_n$ (**I**)

The complex was synthesized from the reaction mixture of pyridine-2,6-dicarboxylic acid (83.6 mg, 0.5 mmol), cerium sulfate (201.7 mg, 0.5 mmol) and water (10 mL). The mixture was homogenized by stirring for 30 min, then transferred into 20 mL Teflon-lined stainless steel autoclave under autogenous pressure at 160 °C for 4 days. After cooling the reaction system to room temperature at a rate of 5 °C/h, yellow-green block crystals were isolated. Calcd. for the complex  $\text{C}_{21}\text{H}_{15.50}\text{N}_3\text{O}_{15.25}\text{Ce}_2$  (%C, 30.24; H, 1.87; N, 5.04%. Found: C, 30.19; H, 1.92; N, 4.78%, 3431(br), 1619(s), 1587(s), 1568(s), 1444(s), 1392(s), 1361(s), 1290(m), 1278(m), 762(m), 730(m), 1178(w), 1077(w), 1018(w), 926(w), 829(w), 762(w), 697(w), 660(w), 595(w), 524(w), 432(w).

### 2.2.2. Synthesis of $\{[\text{Ce}_2(\text{PDA})_2(\text{H}_2\text{O})_5\text{SO}_4] \cdot 2\text{H}_2\text{O}\}_n$ (**II**)

A mixture of pyridine-2,6-dicarboxylic acid (83.6 mg, 0.5 mmol), cerium sulfate (201.7 mg, 0.5 mmol) and water (10 mL) was homogenized by stirring for 30 min, then transferred into 25 mL Teflon-lined stainless steel autoclave under autogenous pressure at 160 °C for 3 days. After cooling the reaction system to room temperature at a rate of 5 °C/h, clear block crystals were isolated. Calc.

for  $\text{C}_{14}\text{H}_6\text{N}_2\text{O}_{19}\text{Ce}_2\text{S}$  (%): C, 20.54; H, 0.74; N, 3.42. Found: C, 20.51; H, 0.76; N, 3.45. IR data (KBr pellet,  $\text{cm}^{-1}$ ): 3424(b), 3086(w), 1623(s), 1592(s), 1560(s), 1477(w), 1438(s), 1389(s), 1367(m), 1277(m), 1160(m), 1125(s), 1095(s), 1077(s), 1014(m), 978(w), 930(m), 863(w), 846(w), 821(w), 772(m), 741(m), 729(m), 699(m), 655(m), 607(m), 523(w), 465(w), 433(m).

## 3. Results and discussion

### 3.1. The IR spectra of the complexes

Complexes **I** and **II** are stable in the solid state upon exposure to air and insoluble in common solvents such as  $\text{CH}_3\text{COCH}_3$ ,  $\text{CH}_3\text{CH}_2\text{OH}$ ,  $\text{CH}_3\text{OH}$ ,  $\text{CHCl}_3$ ,  $\text{CHCl}_2$ ,  $\text{CH}_3\text{CN}$ , THF or DMF. The broad bands around 3436 and 3424  $\text{cm}^{-1}$  and peaks at 926 and 928  $\text{cm}^{-1}$  in complexes **I** and **II** are due to water molecules in coordination and lattice forms [38,39]. The strong infrared absorption bands at about 1620 and 1380  $\text{cm}^{-1}$  in complex **I** and 1621 and 1388  $\text{cm}^{-1}$  in complex **II** are contributed to the coordinated carboxylates [40]. The IR absorption bands at 1563 and 729  $\text{cm}^{-1}$  in complex **I** and 1592 and 729 in complex **II** represent the characteristic skeleton vibrations of the pyridine ring. In complex **I**, the  $\delta_{\text{O}-\text{C}-\text{O}}$  vibration in plane occurs as sharp peaks in the range of 660–760  $\text{cm}^{-1}$ . The absence of the characteristic bands ranging from 1690 to 1730  $\text{cm}^{-1}$  indicates that the  $\text{H}_2\text{PDA}$  ligands are completely deprotonated in the form of  $\text{PDA}^{2-}$  anions upon reaction with the metal ions [41]. In complex **II**, the absorptions related to the  $\text{SO}_4^{2-}$  ions are also presented in the infrared spectrum. Three bands appearing at 607, 655, and 699  $\text{cm}^{-1}$  are particularly evident for the  $\nu_4$  mode of  $\text{SO}_4^{2-}$ , and three bands at higher wave numbers (1159, 1189, and 1277  $\text{cm}^{-1}$ ) could be related to  $\nu_3$ . The two bands observed at 1013 and 929  $\text{cm}^{-1}$  reflect the  $\nu_1$  stretching mode of  $\text{SO}_4^{2-}$ , the one at 929  $\text{cm}^{-1}$  may be assigned to either  $\nu_1$  or  $\nu_3$  [8]. The absorption related to the Ce–N and Ce–O stretching vibrations of the complexes were observed at 523–433  $\text{cm}^{-1}$  [38,39].

**Table 1**  
Summary of crystallographic data for the complexes.

Compound	<b>I</b>	<b>II</b>
Empirical formula	$\text{C}_{21}\text{H}_{15.50}\text{N}_3\text{O}_{15.25}\text{Ce}_2$	$\text{C}_{14}\text{H}_6\text{N}_2\text{O}_{19}\text{Ce}_2\text{S}$
Formula weight	834.10	818.51
Temperature (K)	296(2)	296(2)
Wavelength (Å)	0.71073	0.71073
Crystal system	Monoclinic	Orthorhombic
Space group	P21/c	Pna21
<i>a</i> Å	11.0071(9)	18.754
<i>b</i> Å	17.5297(15)	6.5583(16)
<i>c</i> Å	13.4570(12)	18.754(5)
$\alpha^\circ$	90	90
$\beta^\circ$	100.9820(10)	90
$\gamma^\circ$	90	90
<i>Z</i>	4	4
Density(calculated)	2.174 $\text{Mg/m}^3$	2.357 $\text{Mg/m}^3$
<i>F</i> (000)	1602	1552
Crystal size/ $\text{mm}^3$	0.51 × 0.40 × 0.36	0.40 × 0.28 × 0.20
Range for data collection/ $^\circ$	1.88 to 25.00	2.43 to 25.00
Limiting indices	$-11 \leq h \leq 13, -18 \leq k \leq 20, -15 \leq l \leq 15$	$-22 \leq h \leq 22, -7 \leq k \leq 7, -19 \leq l \leq 22$
Reflections collected/unique	12628/4488 [ $R_{\text{int}} = 0.0205$ ]	28874/5124 [ $R_{\text{int}} = 0.0268$ ]
Refinement method	Full-matrix least-squares on $F^2$	Full-matrix least-squares on $F^2$
Data/restraints/parameters	4488/0/379	2663/1/344
Goodness-of-fit on $F^2$	1.050	0.0814
Volume $\text{Å}^3$	2549.0(4)	2306.6(9)
Final <i>R</i> indices [ $I > 2\sigma(I)$ ]	$R_1 = 0.0226, wR_2 = 0.0582$	$R_1 = 0.0316, wR_2 = 0.0635$
<i>R</i> indices (all data)	$R_1 = 0.0269, wR_2 = 0.0597$	$R_1 = 0.0365, wR_2 = 0.0646$
Largest diff. peak and hole/ $(\text{e} \cdot \text{Å}^{-3})$	0.644 and $-0.729$	0.911 and $-0.799$

**Table 2**  
Selected bond lengths(Å) and bond angles(°) for the complexes.

<b>Bond lengths</b>					
<b>I</b>					
Ce(1)–O(1)	2.353(3)	Ce(2)–O(11)	2.466(3)		
Ce(1)–O(8)	2.369(3)	Ce(2)–O(7)	2.491(2)		
Ce(1)–O(9)	2.396(3)	Ce(2)–O(10)	2.548(2)		
Ce(1)–O(2)	2.478(3)	Ce(2)–O(6)	2.561(3)		
Ce(1)–O(2W)	2.494(3)	Ce(2)–O(6) <sup>a</sup>	2.579(2)		
Ce(1)–O(3)	2.535(2)	Ce(2)–O(1W)	2.590(3)		
Ce(1)–O(3W)	2.561(3)	Ce(2)–N(3)	2.608(3)		
Ce(1)–N(1)	2.593(3)	Ce(2)–N(2)	2.643(3)		
Ce(2)–O(4)	2.463(2)				
<b>II</b>					
Ce(1)–O(17)	2.349(8)	Ce(1)–O(3)	2.919(7)	Ce(2)–O(10)	2.635(7)
Ce(1)–O(16)	2.492(8)	Ce(1)–O(1)	2.928(9)	Ce(2)–N(2)	2.643(11)
Ce(1)–O(14)	2.537(8)	Ce(2)–O(13)	2.619(7)	Ce(2)–O(11)	2.671(7)
Ce(1)–O(4)	2.540(9)	Ce(2)–O(6)	2.455(9)	Ce(2)–N(1)	2.691(11)
Ce(1)–O(15)	2.541(8)	Ce(2)–O(2)	2.504(8)	Ce(2)–O(12)	2.716(7)
Ce(1)–O(18)	2.551(9)	Ce(2)–O(3)	2.569(7)	Ce(1)–O(7)	2.669(8)
Ce(1)–O(2)	2.574(7)	Ce(2)–O(7)	2.610(8)	Ce(2)–O(13)	2.619(7)
<b>Bond lengths</b>					
<b>I</b>					
O(1)–Ce(1)–O(8)	100.09(12)	O(11)–Ce(2)–O(10)	123.75(8)		
O(1)–Ce(1)–O(9)	85.57(11)	O(7)–Ce(2)–O(10)	83.12(9)		
O(8)–Ce(1)–O(9)	152.88(10)	O(4)–Ce(2)–O(6)	84.04(8)		
O(1)–Ce(1)–O(2)	162.10(10)	O(11)–Ce(2)–O(6)	154.99(9)		
O(8)–Ce(1)–O(2)	89.82(10)	O(7)–Ce(2)–O(6)	122.45(8)		
O(9)–Ce(1)–O(2)	92.39(10)	O(10)–Ce(2)–O(6)	76.85(8)		
O(1)–Ce(1)–O(2W)	89.91(12)	O(4)–Ce(2)–O(6) <sup>a</sup>	129.80(8)		
O(8)–Ce(1)–O(2W)	132.99(10)	O(11)–Ce(2)–O(6) <sup>a</sup>	107.29(8)		
O(9)–Ce(1)–O(2W)	72.98(11)	O(7)–Ce(2)–O(6) <sup>a</sup>	150.53(8)		
O(2)–Ce(1)–O(2W)	72.53(11)	O(10)–Ce(2)–O(6) <sup>a</sup>	69.96(8)		
O(1)–Ce(1)–O(3)	72.94(9)	O(6)–Ce(2)–O(6) <sup>a</sup>	63.75(9)		
O(8)–Ce(1)–O(3)	78.55(9)	O(4)–Ce(2)–O(1W)	70.91(8)		
O(9)–Ce(1)–O(3)	77.85(10)	O(11)–Ce(2)–O(1W)	74.08(8)		
O(2)–Ce(1)–O(3)	124.03(8)	O(7)–Ce(2)–O(1W)	139.65(9)		
O(2W)–Ce(1)–O(3)	147.17(10)	O(10)–Ce(2)–O(1W)	136.79(8)		
O(1)–Ce(1)–O(3W)	77.57(10)	O(6)–Ce(2)–O(1W)	77.02(8)		
O(8)–Ce(1)–O(3W)	69.16(9)	O(6) <sup>a</sup> –Ce(2)–O(1W)	67.01(8)		
O(9)–Ce(1)–O(3W)	137.65(10)	O(4)–Ce(2)–N(3)	140.93(9)		
O(2)–Ce(1)–O(3W)	92.33(9)	O(11)–Ce(2)–N(3)	62.47(9)		
O(2W)–Ce(1)–O(3W)	68.49(10)	O(7)–Ce(2)–N(3)	72.77(9)		
O(3)–Ce(1)–O(3W)	131.06(9)	O(10)–Ce(2)–N(3)	61.40(9)		
O(1)–Ce(1)–N(1)	134.06(10)	O(6)–Ce(2)–N(3)	134.08(9)		
O(8)–Ce(1)–N(1)	77.68(10)	O(6) <sup>a</sup> –Ce(2)–N(3)	83.64(8)		
O(9)–Ce(1)–N(1)	79.44(10)	O(1W)–Ce(2)–N(3)	116.36(8)		
O(2)–Ce(1)–N(1)	62.48(9)	O(4)–Ce(2)–N(2)	70.14(9)		
O(2W)–Ce(1)–N(1)	125.42(11)	O(11)–Ce(2)–N(2)	135.38(9)		
O(3)–Ce(1)–N(1)	61.56(9)	O(7)–Ce(2)–N(2)	61.80(9)		
O(3W)–Ce(1)–N(1)	138.37(9)	O(10)–Ce(2)–N(2)	70.90(8)		
O(4)–Ce(2)–O(11)	85.63(9)	O(6)–Ce(2)–N(2)	60.69(8)		
O(4)–Ce(2)–O(7)	79.01(8)	O(6) <sup>a</sup> –Ce(2)–N(2)	117.07(8)		
O(11)–Ce(2)–O(7)	77.48(9)	O(1W)–Ce(2)–N(2)	127.10(8)		
O(4)–Ce(2)–O(10)	141.04(8)	N(3)–Ce(2)–N(2)	116.49(9)		
<b>II</b>					
O(17)–Ce(1)–O(16)	124.9(3)	O(14)–Ce(1)–O(3)	69.0(2)	O(6)–Ce(2)–N(2)	60.7(3)
O(17)–Ce(1)–O(14)	129.6(2)	O(4)–Ce(1)–O(3)	46.9(2)	O(2)–Ce(2)–N(2)	116.9(3)
O(16)–Ce(1)–O(14)	71.3(3)	O(15)–Ce(1)–O(3)	97.9(2)	O(3)–Ce(2)–N(2)	123.6(3)
O(17)–Ce(1)–O(4)	90.8(3)	O(18)–Ce(1)–O(3)	67.8(2)	O(7)–Ce(2)–N(2)	59.9(3)
O(16)–Ce(1)–O(4)	140.1(3)	O(2)–Ce(1)–O(3)	156.4(3)	O(13)–Ce(2)–N(2)	72.1(3)
O(14)–Ce(1)–O(4)	71.9(3)	O(7)–Ce(1)–O(3)	137.8(3)	O(10)–Ce(2)–N(2)	109.2(3)
O(17)–Ce(1)–O(15)	73.0(2)	O(17)–Ce(1)–O(1)	140.6(2)	O(6)–Ce(2)–O(11)	77.4(3)
O(16)–Ce(1)–O(15)	134.0(3)	O(16)–Ce(1)–O(1)	89.5(3)	O(2)–Ce(2)–O(11)	128.9(3)
O(14)–Ce(1)–O(15)	134.1(3)	O(14)–Ce(1)–O(1)	75.4(3)	O(3)–Ce(2)–O(11)	71.5(2)
O(4)–Ce(1)–O(15)	68.2(3)	O(6)–Ce(2)–O(2)	153.2(2)	O(7)–Ce(2)–O(11)	88.6(2)
O(17)–Ce(1)–O(18)	70.6(2)	O(6)–Ce(2)–O(3)	70.1(3)	O(13)–Ce(2)–O(1)	144.5(3)
O(16)–Ce(1)–O(18)	69.9(3)	O(2)–Ce(2)–O(3)	119.5(3)	O(10)–Ce(2)–O(1)	152.9(2)
O(14)–Ce(1)–O(18)	73.9(3)	O(6)–Ce(2)–O(7)	120.5(3)	N(2)–Ce(2)–O(11)	72.5(3)
O(4)–Ce(1)–O(18)	113.2(3)	O(2)–Ce(2)–O(7)	62.4(3)	O(6)–Ce(2)–N(1)	121.6(3)
O(15)–Ce(1)–O(18)	143.5(3)	O(3)–Ce(2)–O(7)	155.4(2)	O(2)–Ce(2)–N(1)	60.0(3)
O(17)–Ce(1)–O(2)	124.9(2)	O(3)–Ce(1)–O(1)	110.9(2)	O(3)–Ce(2)–N(1)	59.6(2)
O(16)–Ce(1)–O(2)	66.9(3)	O(4)–Ce(1)–O(1)	66.7(3)	O(7)–Ce(2)–N(1)	117.6(3)
O(14)–Ce(1)–O(2)	105.4(3)	O(15)–Ce(1)–O(1)	68.8(3)	O(13)–Ce(2)–N(1)	105.6(3)
O(4)–Ce(1)–O(2)	109.6(3)	O(18)–Ce(1)–O(1)	147.2(3)	O(10)–Ce(2)–N(1)	71.3(3)
O(15)–Ce(1)–O(2)	69.0(3)	O(2)–Ce(1)–O(1)	46.7(2)	N(2)–Ce(2)–N(1)	176.8(3)

(continued on next page)

Table 2 (continued)

O(18)-Ce(1)-O(2)	134.1(3)	O(7)-Ce(1)-O(1)	106.5(2)	O(11)-Ce(2)-N(1)	109.8(3)
O(17)-Ce(1)-O(7)	73.7(2)	O(6)-Ce(2)-O(13)	83.0(3)	O(6)-Ce(2)-O(12)	71.4(3)
O(16)-Ce(1)-O(7)	69.9(3)	O(2)-Ce(2)-O(13)	71.6(3)	O(2)-Ce(2)-O(12)	85.8(3)
O(14)-Ce(1)-O(7)	141.1(3)	O(3)-Ce(2)-O(13)	128.3(2)	O(3)-Ce(2)-O(12)	77.3(2)
O(4)-Ce(1)-O(7)	145.7(3)	O(7)-Ce(2)-O(13)	76.3(2)	O(7)-Ce(2)-O(12)	126.4(2)
O(15)-Ce(1)-O(7)	78.0(3)	O(6)-Ce(2)-O(10)	128.2(3)	O(13)-Ce(2)-O(1)	52.1(2)
O(18)-Ce(1)-O(7)	90.6(3)	O(2)-Ce(2)-O(10)	78.5(2)	O(10)-Ce(2)-O(1)	141.7(3)
O(2)-Ce(1)-O(7)	60.7(3)	O(3)-Ce(2)-O(10)	80.4(2)	N(2)-Ce(2)-O(12)	109.1(3)
O(17)-Ce(1)-O(3)	65.2(2)	O(7)-Ce(2)-O(10)	75.9(2)	O(11)-Ce(2)-O(1)	141.6(2)
O(16)-Ce(1)-O(3)	128.0(2)	O(13)-Ce(2)-O(1)	146.1(2)	N(1)-Ce(2)-O(12)	70.6(3)

Symmetry transformations used to generate equivalent atoms for complex I.

<sup>a</sup>  $-x + 1, -y + 1, -z$ .

### 3.2. X-ray structures of complexes

#### 3.2.1. X-ray crystallographic analysis and data collection

Single-crystal diffraction data **I** and **II** were collected from suitable single crystals of the complexes on a Bruker Smart CCD X-ray single-crystal diffractometer with graphite monochromated MoK $\alpha$ -radiation ( $\lambda = 0.71073$  Å) at 296(2) K. All independent reflections were collected in a range of 1.88–25.00° for complex **I** and 2.43–25.00° for complex **II** (determined in the subsequent refinement). Multi-scan empirical absorption corrections were applied to the data using SADABS. The crystal structure was solved by direct methods and Fourier synthesis. Positional and thermal parameters were refined by the full-matrix least-squares method on  $F^2$  using the SHELXTL software package. The final least-square cycle of refinement gave  $R_1 = 0.0226$ ,  $wR_2 = 0.0582$  for **I** and  $R_1 = 0.0316$ ,  $wR_2 = 0.0635$  for **II**, the weighting scheme  $w = 1/[\sigma^2(F_0^2) + (0.1999P)^2 + 0.0000P]$ , for complex **I** and  $w = 1/[\sigma^2(F_0^2) + (0.0000P)^2 + 0.0000P]$  for complex **II**, where  $P = (F_0^2 + 2F_c^2)/3$ . The crystallographic data, selected bond lengths and bond angles for complexes **I** and **II** are listed in Tables 1 and 2, respectively.

#### 3.2.2. Structure analysis of I

The single-crystal analyses reveal that complex **I** exhibits a binuclear cerium entity connected by carboxylic oxygen with two types of coordination environments (see Fig. 1a). Namely, Ce1 shows 8-coordination with the N<sub>1</sub>O<sub>7</sub> donor and Ce2 shows 9-coordination with the N<sub>2</sub>O<sub>7</sub> donor, respectively (see Fig. 1b and c). Four kinds of coordination modes a, b, c and d exist in the structure (see Scheme 1). The Ce1 ion shows 8-coordination with

distorted trigonal dodecahedron, four PDA anions act as one tetradentate mode (a mode) and three pentadentate modes (two of them adopting c mode, one of them adopting d mode) and two molecules of water. The Ce2 ion shows 9-coordination with a tricapped trigonal prism, four PDA anions act as two tetradentate modes (b mode) and two pentadentate modes (d mode and c mode). The framework of **I** is built upon the building block of Ce<sub>4</sub>(CO<sub>2</sub>)<sub>4</sub> unit (18-membered ring) among which the neighboring Ce ions are linked by O–C–O groups in  $\mu_2$ -bridging fashion, and Ce2 and Ce2A are bridged by O6 and O6A using  $\mu_2$ -bridging fashion, in which an approximate rhombic Ce2O2 (Ce2–O6–Ce2A–O6A) grid is observed with the distance Ce2...Ce2A of 4.365(2) Å and the corresponding interior angles of 63.75(9)° for  $\angle$  O6–Ce2–O6A and  $\angle$  O6–Ce2A–O6A, 116.24(1)° for  $\angle$  Ce2–O6–Ce2A  $\angle$  Ce2–O6A–Ce2A, respectively (see Fig. 2a). The adjacent tetranuclear homometallic Ce<sub>4</sub>(CO<sub>2</sub>)<sub>4</sub> units with 18-membered motifs assembled by two carboxylate bridges (O–C–O) to propagate an infinite 1D chain (Fig. 2b) and the neighboring chains are connected via carboxylate bridges (O–C–O) to form a 2D layer (Fig. 2c), which are further linked up and down through hydrogen bonds (O–H...O) (see Table 3) to construct a 3D polymer architecture, as illustrated in Fig. 3. It is noteworthy that within the 2D homonuclear layer, octagonal rings (O12–H3WB–O3W–H3WA–O12'–H3WB'–O3W'–H3WA'–O12) constructed from coordinated water molecules and O atoms from different ligands among the building blocks of Ce<sub>4</sub>(CO<sub>2</sub>)<sub>4</sub> above and below the middle layer (Fig. 3). Obviously, these intralayer weak interactions contribute to the additional stability of the 3D structure [42].

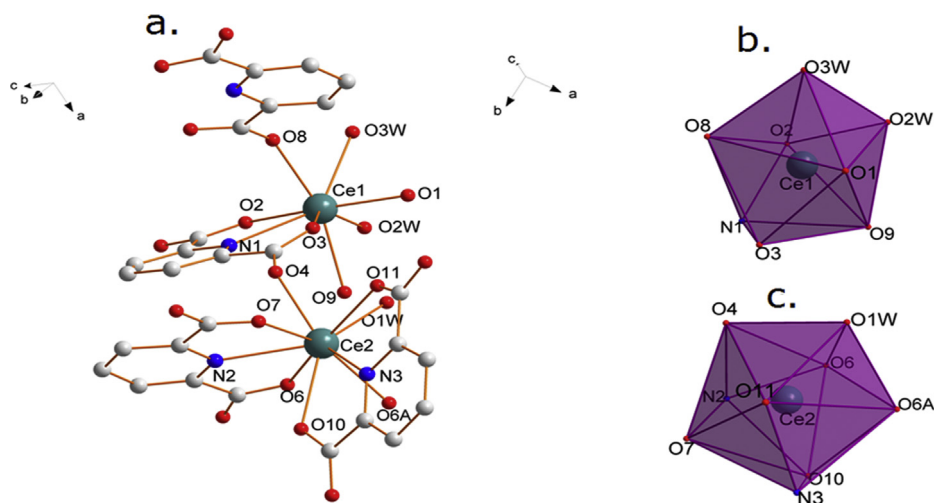
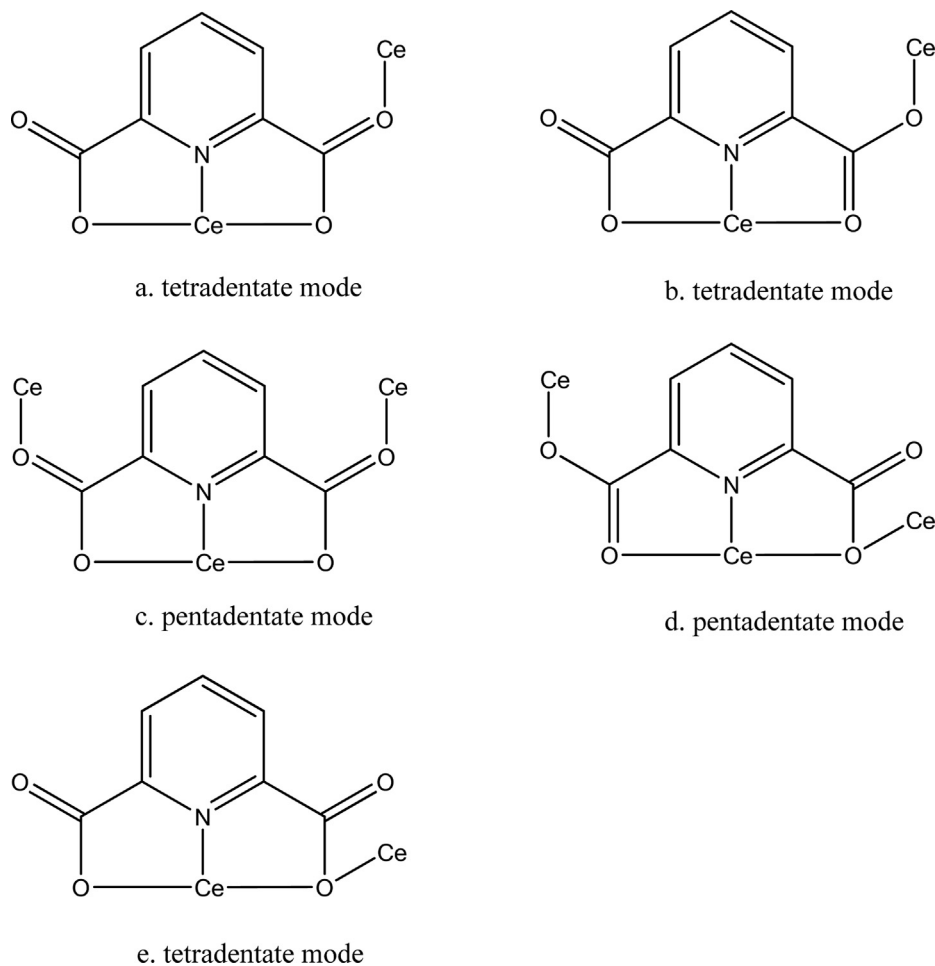


Fig. 1. (a) Coordination environment of complex **I**; the asymmetric unit and the related coordination atoms are labeled; lattice water and hydrogen atoms are omitted for clarity. (b) Highlight of the coordination polyhedra for the two crystallographically independent Ce(IV) ions.



**Scheme 1.** Typical coordination modes of the  $\text{PDA}^{2-}$  anions in the complexes.

### 3.2.3. Structure analysis of **II**

The molecular structure of complex **II** is shown in Fig. 4, exhibiting a binuclear cerium entity connected by carboxylic oxygen with two types of coordination environments, namely, Ce1 shows eight-coordination with the  $\text{O}_8$  donor set, while Ce2 shows ten-coordination with the  $\text{N}_2\text{O}_8$  donor set, respectively. Two kinds of coordination modes b and e exist in the structure (see Scheme 1). Five molecules of water together with three carboxylic oxygen

atoms make up the coordination sphere of the Ce1 center with a geometry of dodecahedron. The Ce2 ion shows 10-coordinated environment with a double-capped cubic prism configuration, where two  $\text{PDA}^{2-}$  anions adopt one tetradentate (b mode) and one adopts tetradentate (e mode) ligands chelating to Ce2 occupying six coordination sites of the Ce2 ion, and two sulfate anions act as bidentate fashion to fill the remaining four coordination sites. Unchelated PDA ligands around Ce1 ion are observed. The Ce–O

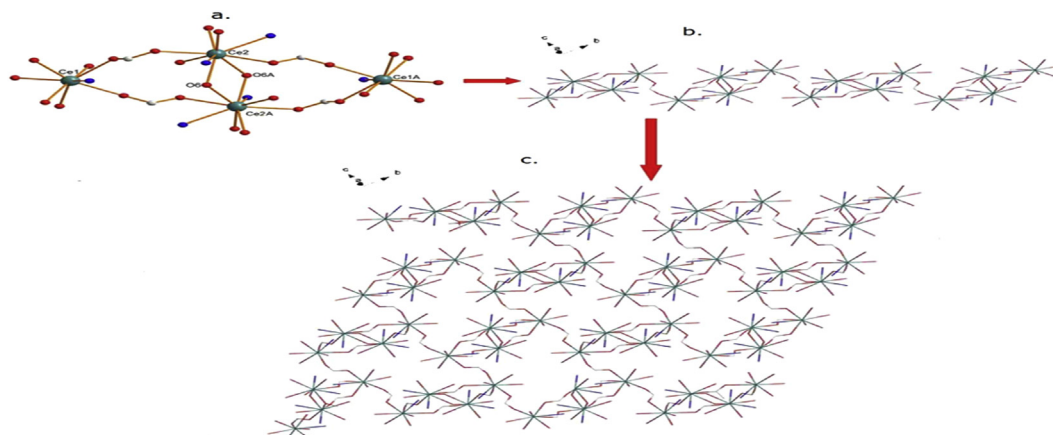


**Fig. 2.** (a) Diagram showing the building block of the coordination polymer (lattice water molecules and hydrogen atoms are omitted for clarity), (b) figure showing the 1D sinusoid-shaped  $(\text{Ce-OCO-Ce-O}_2\text{-Ce-OCO-Ce})_\infty$  chain, (c) view of the 2D packing structure of the polymer.

**Table 3**  
Hydrogen bond geometry (Å) in the complex I.

D-H...A	d(D-H)	d(H...A)	d(D...A)	∠(DHA)
O(4W)–H(4WA)...O(4W) <sup>d</sup>	0.85	2.14	2.760(3)	129.9
O(3W)–H(3WB)...O(12) <sup>c</sup>	0.85	1.95	2.793(4)	171.5
O(3W)–H(3WA)...O(12) <sup>e</sup>	0.85	2.18	2.905(4)	142.8
O(2W)–H(2WB)...O(1W) <sup>c</sup>	0.85	2.48	3.087(4)	129.2
O(2W)–H(2WB)...O(5) <sup>f</sup>	0.85	2.45	2.914(5)	115.2
O(2W)–H(2WA)...O(4W)	0.85	1.98	2.811(13)	165.9
O(1W)–H(1WB)...O(2) <sup>b</sup>	0.85	2.59	3.153(4)	124.3
O(1W)–H(1WB)...O(3)	0.85	2.14	2.870(4)	144.2
O(1W)–H(1WA)...O(10) <sup>a</sup>	0.85	1.96	2.806(4)	170.7

Symmetry transformations used to generate equivalent atoms.

<sup>a</sup>  $-x + 1, -y + 1, -z$ .

<sup>b</sup>  $x, -y + 1/2, z - 1/2$ .

<sup>c</sup>  $x, -y + 1/2, z + 1/2$ .

<sup>d</sup>  $-x + 1, -y, -z$ .

<sup>e</sup>  $-x, y - 1/2, -z - 1/2$ .

<sup>f</sup>  $-x + 1, y - 1/2, -z + 1/2$ .

bond lengths are from 2.349(8) to 2.928(9) Å (Table 2), while the bond lengths of Ce–N are from 2.643(1) to 2.691(1) Å. The bond length observation in the present work is consistent with the previous work for the lanthanide involved polymers [9]. The average bond length of Ce–O<sub>PDA</sub> is longer than that of Ce–O<sub>W</sub>. It is noteworthy that the bond distances of Ce...S1 and Ce...S1A are 3.283(2) and 3.276(2) Å, respectively, which is particularly rare in the similar complexes, considering the sum of the van der Waals radii of Ce and S atoms, which is slightly longer than 3.4 Å. As a result, it is reasonable to assume that there is certain interaction between Ce and S atoms [43]. The dihedral angle between pyridine rings connected to the Ce2 centers is 24.29(4)°, which is a small deviation from the coplanar case. Actually, from the point view of stereochemical effects, the closer the dihedral angle is to 90°, the more stable the configuration of complex II. Obviously, the chelating coordination of SO<sub>4</sub><sup>2-</sup> anions to Ce2 ion from both above and below defines the certain dihedral angle. Two sets of oxygen atoms of the SO<sub>4</sub><sup>2-</sup> anion in I, namely, (O10, O11) and (O12, O13), in company with S1 atom define two planes with a dihedral angle of nearly 90° between them (88.94(3)°), and the bond lengths of S–O are nearly equal (1.446(9)–1.471(8)Å). The angles of ∠O–S–O in a sulfate anion are slightly deviated from those of an ideal tetrahedron, which are sufficient to reduce the local environmental symmetry from T<sub>d</sub> to C<sub>2v</sub> for the S atom [40].

The coordination polymer II consists of the building block of [Ce<sub>2</sub>(PDA)(HPDA)(H<sub>2</sub>O)<sub>5</sub>SO<sub>4</sub>]<sub>2</sub>·2H<sub>2</sub>O(II). Ce1 and Ce2 are connected through two carboxylic oxygen (O2, O7) from two PDA<sup>2-</sup> ligands.

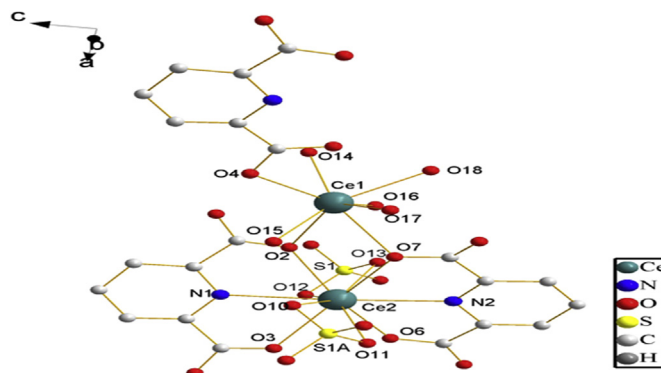


**Fig. 4.** Coordination environment of complex II; the asymmetric unit and the related coordination atoms are labeled; lattice water and hydrogen atoms are omitted for clarity.

The bond lengths are 2.574(7) Å for Ce1–O2, 2.669(8) Å for Ce1–O7, 2.504(8) Å for Ce2–O2 and 2.610(8) Å for Ce2–O7. Consequently, an approximate rhombic Ce<sub>2</sub>O<sub>2</sub> grid is formed with the corresponding angles of 60.65(2)° for ∠O2–Ce1–O7, 62.36(2)° for ∠O2–Ce2–O7, 122.02(3)° for ∠Ce1–O2–Ce2 and 114.55(3)° for ∠Ce1–O7–Ce2, respectively. Two Ce(IV) ions are well-separated with the distance of 4.441(8) Å (Ce1...Ce2). The coordination polymer is connected between the adjacent building block of [Ce<sub>2</sub>(PDA)(HPDA)(H<sub>2</sub>O)<sub>5</sub>SO<sub>4</sub>]<sub>2</sub>·2H<sub>2</sub>O through carboxylate bridges (O–C–O). An infinite 1D (Ce–O<sub>2</sub>–Ce–OCO–Ce–O<sub>2</sub>–Ce)<sub>∞</sub> wavelike chain motif along the *a* axis is formed through the bridges of carboxylate (O–C–O) and double oxygen alternately. The distances between Ce–O<sub>2</sub>–Ce, Ce–OCO–Ce and Ce–OSO–Ce are observed as 4.441(8), 5.264(8) and 6.558(2) Å in the 1D chain, respectively. Furthermore, the adjacent 1D chains are jointed through SO<sub>4</sub><sup>2-</sup> anions from both above and below to construct a highly ordered 2D layer along the *c* axis [8], as illustrated in Fig. 5. The repeat unit in the 2D layer represents a motif consisting of a hexanuclear homometallic 20-membered Ce<sub>6</sub>C<sub>2</sub>O<sub>10</sub>S<sub>2</sub> ring with a size of 10.665(1) Å × 12.350(2) Å (distances of diagonals). In addition, the parallel pyridine rings of PDA<sup>2-</sup> ligands between adjacent 2D layers are partly overlapped (zipper-like) with distances of 3.556 and 3.505 Å (centroid to centroid distances between the adjacent pyridine rings), which indicate that the strong π–π interactions exist by which the 3D framework is fabricated. The distance between the adjacent layers is 9.506 Å (see Fig. 6). It's noticeable that the Ce(IV) ions, carboxylate oxygen atoms and π–π stacking pyridine rings act

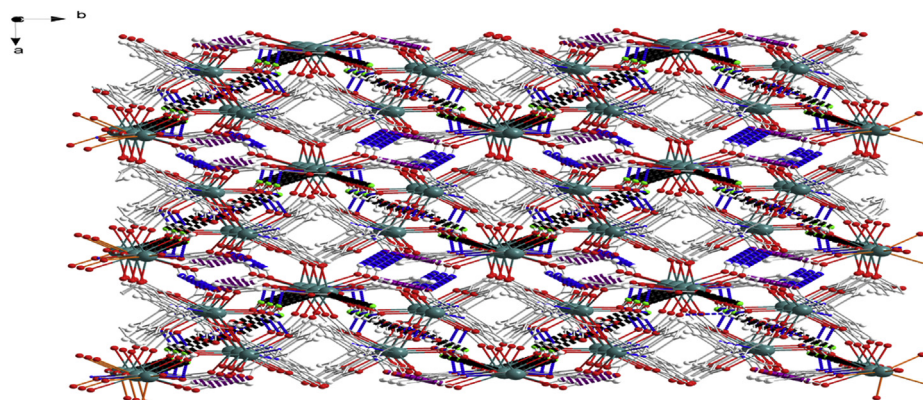


**Fig. 3.** Hydrogen-bonding interactions in complex I presenting 3D network viewed along *c* axis.

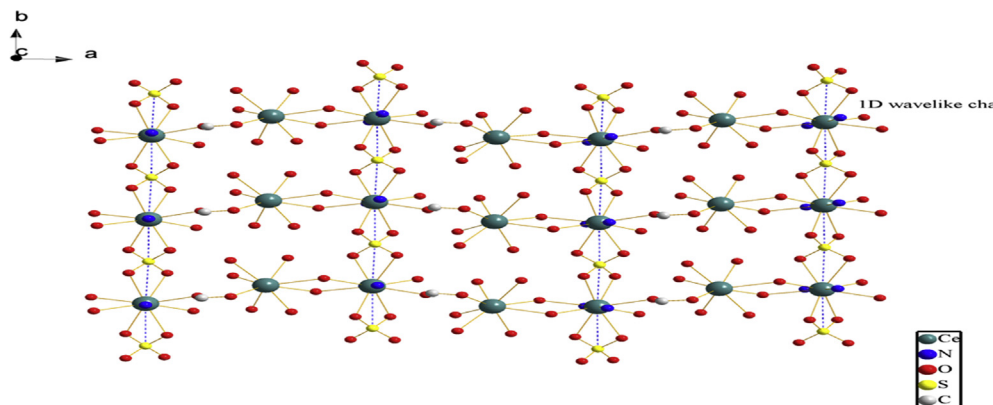


**Fig. 5.** 2D layer of complex **II** constructed by 1D wavelike chains exhibiting the repeat unit consisting of  $Ce_6C_2O_{10}S_2$  ring and the bi-bidentate coordinated mode of  $SO_4^{2-}$  anion;  $Ce \cdots S$  weak interaction. Cyan, Ce; yellow, S; blue, N; red, O; gray, C. (For interpretation of the references to color in this figure legend, the reader is referred to the web version of this article.)

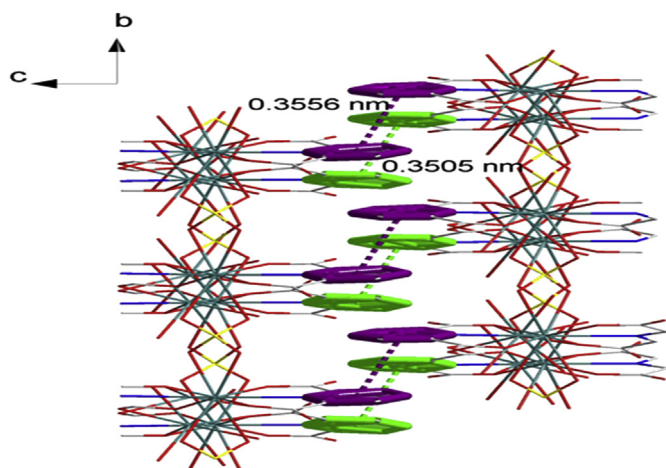


**Fig. 6.** Zipper-like structure in complex **II** constructed by  $\pi$ - $\pi$  stacking interactions. Uncoordinated water and hydrogen atoms were omitted for clarity. Cyan, Ce; yellow, S; blue, N; red, O; gray, C. (For interpretation of the references to color in this figure legend, the reader is referred to the web version of this article.)

as the inner wall of the cavities, inside which the lattice water molecules are occupied. Within the infinite 1D nanosized cavities, the embedded guest water molecules are arranged as linear clusters [29,30], as described in Fig. 7.

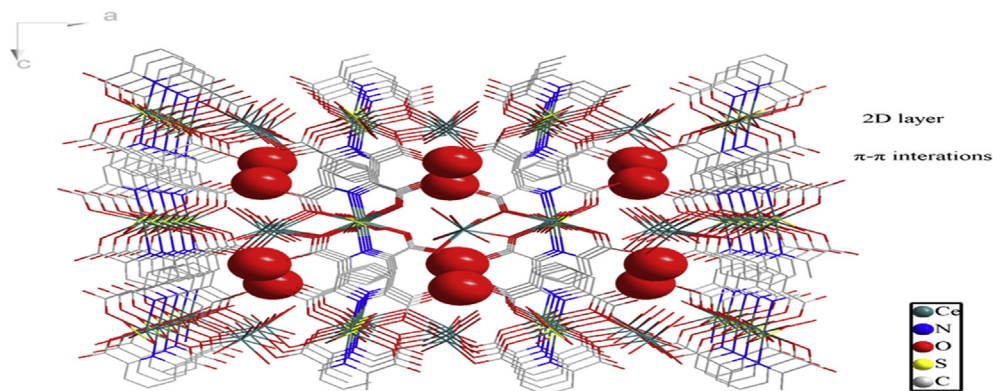


**Fig. 7.** Perspective view of the 3D supramolecular network in complex **II**, highlighting the infinite 1D parallel cavities with guest water molecules being embedded inside (hydrogen atoms were omitted for clarity). Cyan, Ce; yellow, S; blue, N; red, O; gray, C. (For interpretation of the references to color in this figure legend, the reader is referred to the web version of this article.)

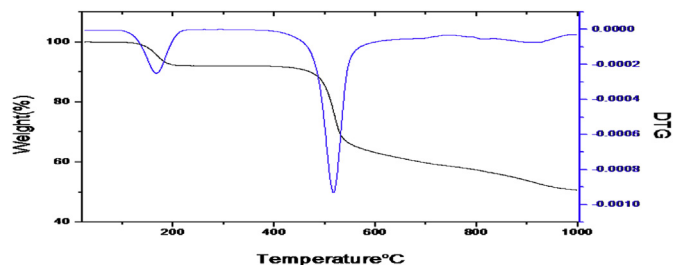


**Fig. 8.** TG and DTG curves of complex **I**.

By comparison, the complex **I** and **II** are different from those of the similar complexes  $\{[Pr_2(PDA)_3(H_2O)_3] \cdot H_2O\}_n$ , and  $\{[Pr_2(PDA)_2(H_2O)_5SO_4] \cdot 2H_2O\}_n$ ,  $H_2PDA =$  pyridine-2,6-dicarboxylic acid) in the corresponding reference in the respects of coordination environments around Ce1 and Ce2, the building blocks and packing diagrams [8,43]. The extent of the difference depends on the stereoelectronic molecular information encoded in the components (i.e., the ligand and the central metal ions) and the external conditions (temperature, solvent system and material ratio).

### 3.3. Thermal analysis

The TG and DTG curves are shown in Fig. 8 and Fig. 9. In the TG and DTG curves of **I**, The first weight loss stage has a decomposition

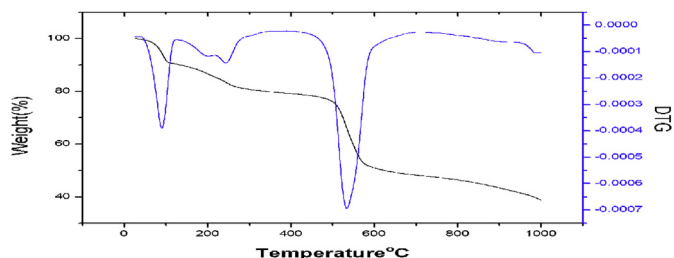


Fig. 9. TG and DTG curves of complex II.

temperature range of 109–230 °C, with a weight loss of 7.69%, which corresponding to the loss of part of three point five molecule of water (theoretical loss is 7.01%). The complex does not decompose until 634 °C which indicates the high thermal stability of its 3D network, and above 634 °C, the complex starts to decompose gradually. Nevertheless the final remnants of 50.72% suggests that the complex does not decomposed completely under the experimental temperature (theoretical residue of  $\text{CeO}_2$  41.34%). The TG and DTG curves of the complex II indicate that the complex decomposes in three steps. The first weight loss stage has a

decomposition temperature range of 25–157 °C, with a weight loss of 10.93% (theoretical loss 10.99%), which can be assigned to the loss of two molecules of lattice water and three molecules of coordinated water. The second weight loss stage has a decomposition temperature range of 157–228 °C, with a weight loss of 4.42%. This can be assigned to the loss of the remaining two coordinated water molecules (theoretical loss is 4.39%). The third weight loss stage has a decomposition temperature range of 400–935 °C, with a weight loss of 42.62%, which is due to the loss of two molecules of  $\text{PDA}^{2-}$  ligands (theoretical loss is 41.05%). The final mass remnant of 42.02% is indicative of deposition of  $\text{CeO}_2$  (theoretical loss is 42.03%).

### 3.4. Luminescent properties

To examine the possibility of modification of the luminescent properties through cations exchange, the solid sample of complex I was immersed in  $\text{CH}_3\text{OH}$  ( $10^{-4}$  M) containing various metal cations to generate solutions at room temperature. Emission spectra of the complex (excited at 225 nm) in the presence of  $\text{Fe}^{3+}$ ,  $\text{Cd}^{2+}$ ,  $\text{Cu}^{2+}$ ,  $\text{Mn}^{2+}$ ,  $\text{Pb}^{2+}$ ,  $\text{Hg}^{2+}$  and  $\text{Zn}^{2+}$  ions with respect to the complex are listed in Fig. 10, respectively. The complex exhibits intense broad emission bands with the maximum at 303 nm upon excitation at

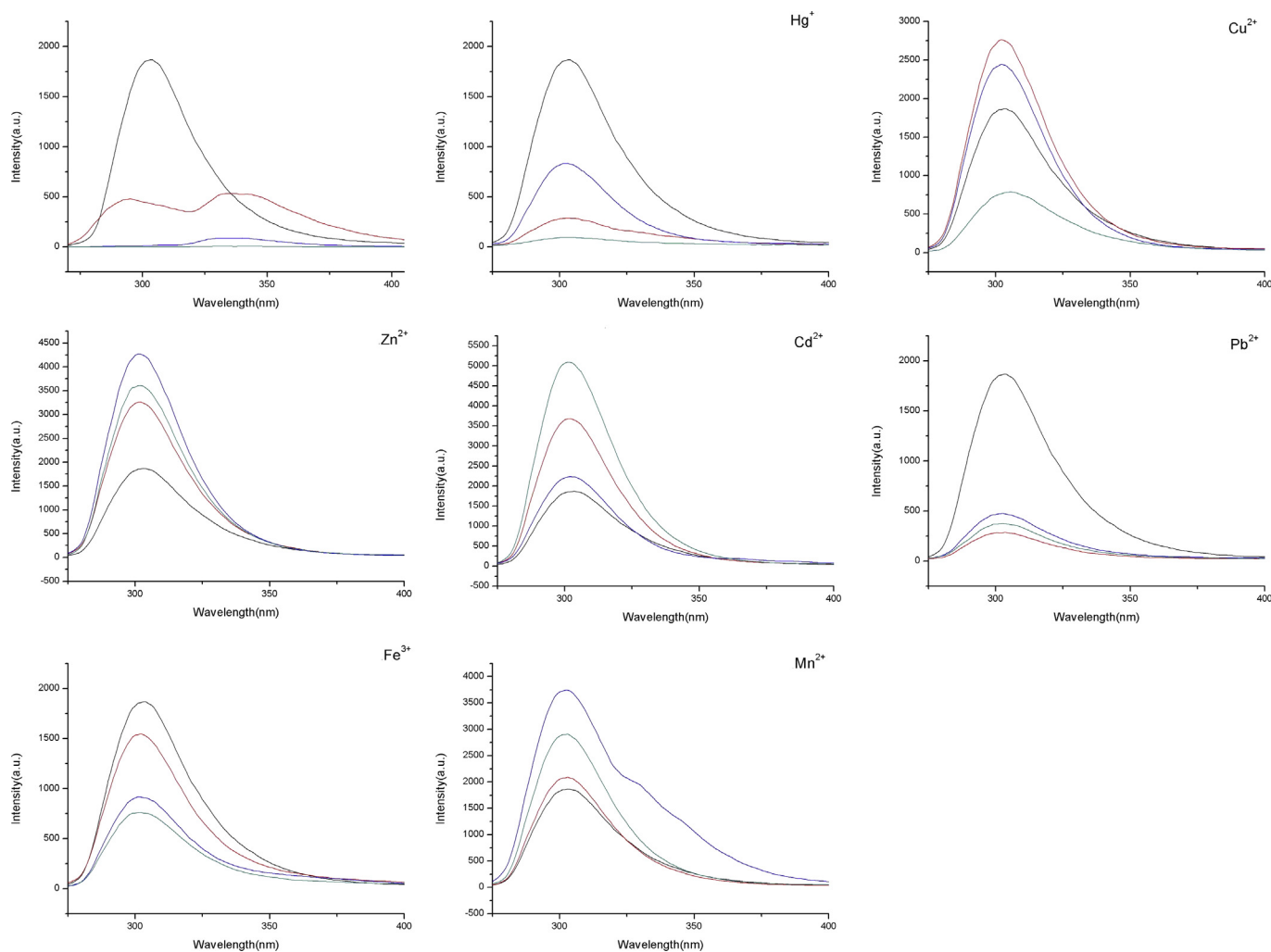


Fig. 10. Luminescent intensity of II at 310 nm in  $\text{CH}_3\text{OH}$  at room temperature upon the addition of  $\text{Hg}^{2+}$ ,  $\text{Cu}^{2+}$ ,  $\text{Ca}^{2+}$ ,  $\text{Zn}^{2+}$ ,  $\text{Cd}^{2+}$ ,  $\text{Pb}^{2+}$ ,  $\text{Fe}^{3+}$  and  $\text{Mn}^{2+}$  ions (excited at 225 nm) (black, no addition; blue,  $10^{-4}$  M; red,  $2 \times 10^{-4}$  M; green,  $3 \times 10^{-4}$  M). (For interpretation of the references to color in this figure legend, the reader is referred to the web version of this article.)



350 nm, which may be due to the  $\pi^* \rightarrow n$  transition. According to the above results, the emission of the complex may be assigned to the ligand-to-metal-charge-transfer bands (LMCT) [19,40,44]. The emission intensity of the complex decreased gradually upon the addition of  $10^{-4}$ – $3 \times 10^{-4}$  M of  $\text{Pb}^{2+}$  ( $\text{Pb}(\text{NO}_3)_2$ ) or  $\text{Fe}^{3+}$  ( $\text{Fe}_2(\text{SO}_4)_3$ ) with respect to the complex. As the concentration of  $\text{Hg}^+$  ( $\text{HgNO}_3$ ) was controlled at  $3 \times 10^{-3}$  M, the emission spectra at 310 nm (excited at 225 nm) for the complex **I** basically quenched. On the contrary, the emission intensities at 303 nm of the complex are significantly enhanced by the presence of  $\text{Cd}^{2+}$  ( $\text{Cd}(\text{CH}_3\text{COO})_2$ ). Interestingly, the significant enhancement of the emission intensity of the complex caused by  $\text{Zn}^{2+}$  or  $\text{Mn}^{2+}$  is much more sensitive to its concentration of  $2 \times 10^{-3}$  M (other than  $10^{-3}$  M and  $3 \times 10^{-3}$  M) than those of any other ions tested at the equivalent concentration, which presents its character of concentration-dependent selectivity, whereas the higher selective concentrations of  $\text{Pb}^{2+}$  are  $10^{-4}$  M and  $2 \times 10^{-3}$  M (as indicated in Fig. 10). The luminescent properties of complex **II** was studied in  $\text{H}_2\text{O}$  ( $10^{-4}$  M) at room temperature. As for complex **II**, when transition metals ( $\text{Cd}^{2+}$ :  $\text{Cd}(\text{CH}_3\text{COO})_2$ ,  $\text{Zn}^{2+}$ :  $\text{Zn}(\text{CH}_3\text{COO})_2$ ,  $\text{Pb}^{2+}$ :  $\text{Pb}(\text{CH}_3\text{COO})_2$ ,  $\text{Hg}^+$ : ( $\text{HgNO}_3$ ),  $\text{Cu}^{2+}$ :  $\text{Cu}(\text{CH}_3\text{COO})_2$ ) are added, the emission intensities at 350 nm (excited at 252 nm) enhanced (Fig. 11). The emission intensities at 351 nm of complex **I** is significantly enhanced in the presence of  $\text{Pb}^{2+}$  ( $2 \times 10^{-4}$  M,  $\text{Pb}(\text{CH}_3\text{COO})_2$ ) ion for about twelve times as strong as that without  $\text{Pb}^{2+}$  ion, while it is enhanced in the presence of  $\text{Cd}^{2+}$  ( $3 \times 10^{-4}$  M,  $\text{Cd}(\text{CH}_3\text{COO})_2$ ) ion for about three times as strong as that without  $\text{Cd}^{2+}$  ion. Strikingly, the significant enhancement of the emission intensity of complex **II** caused by  $\text{Hg}^+$  is much more sensitive to its concentration of  $2 \times 10^{-4}$  M (other than  $10^{-4}$  M and  $3 \times 10^{-4}$  M). The emission intensities of complex **II** increased significantly upon the addition of  $3 \times 10^{-4}$ – $10^{-4}$  M (other than  $10^{-4}$  M– $3 \times 10^{-4}$  M) of  $\text{Zn}^{2+}$ . The mechanism of the luminescent feature of the complexes along with its dependence on the co-existing metal ions is still under investigation.

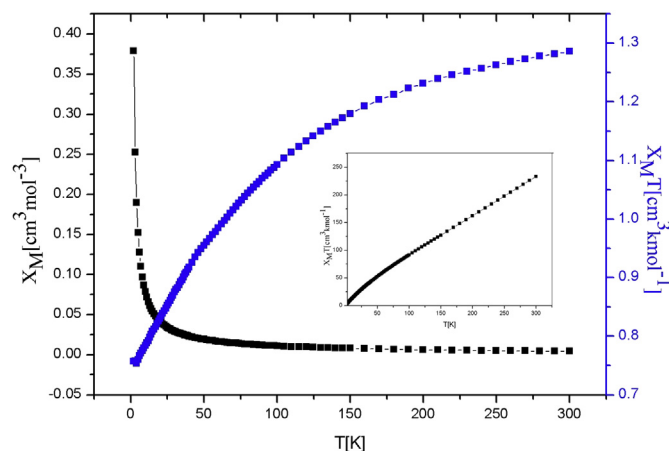


Fig. 12. Thermal variation of  $\chi_M$  and  $\chi_M T$  for compound **II**. Insert: Plot of thermal variation of  $\chi_M^{-1}$  for compound **II**.

### 3.5. Magnetic properties

Variable-temperature magnetic susceptibility of **II** was measured in the 2.0–300 K temperature range. The variation of the inverse of the magnetic susceptibility,  $\chi_M^{-1}$  and  $\chi_M T$  of **II** are shown in Fig. 12. The thermal evolution of  $\chi_M^{-1}$  obeys the Curie–Weiss law,  $\chi_M = C/(T-\theta)$  in the range of 2–300 K with a Weiss constant,  $\theta$ , of  $-14.540$  K and a Curie constant,  $C_M$ , of  $1.311 \text{ cm}^3 \text{ mol}^{-1} \text{ K}$ , respectively. At 300 K, the  $\chi_M T$  value is  $1.286 \text{ cm}^3 \text{ mol}^{-1} \text{ K}$ . On lowering the temperature, the  $\chi_M T$  value decreases smoothly to a minimum of  $0.757 \text{ cm}^3 \text{ mol}^{-1} \text{ K}$  at 2 K. The negative  $\theta$  value and the  $\chi_M T$  vs  $T$  curve reveal typical antiferromagnetic interactions between the Ce(IV) centers. The structural determination indicates that two magnetic

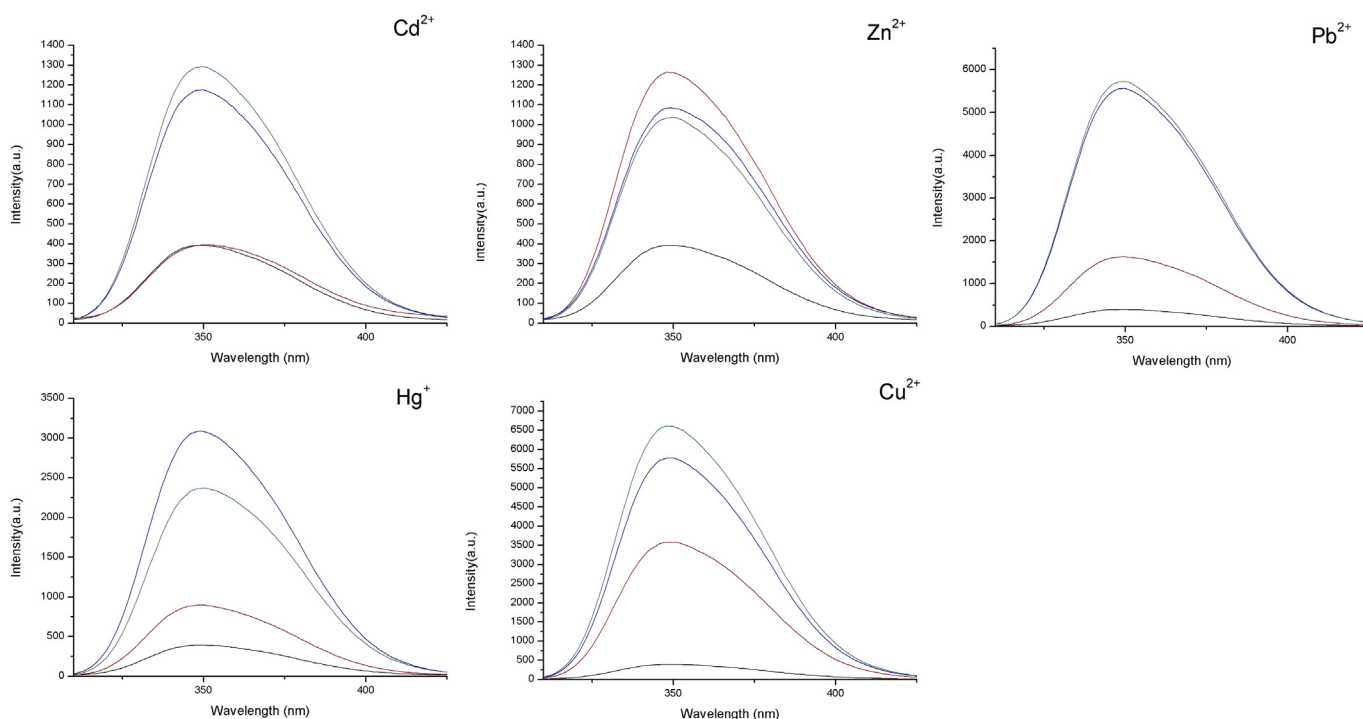


Fig. 11. Luminescent intensity of **II** at 350 nm in  $\text{CH}_3\text{OH}$  at room temperature upon the addition of  $\text{Cd}^{2+}$ ,  $\text{Pb}^{2+}$ ,  $\text{Hg}^+$  and  $\text{Zn}^{2+}$  ions (excited at 252 nm) (black, no addition; blue,  $10^{-4}$  M; red,  $2 \times 10^{-4}$  M; green,  $3 \times 10^{-4}$  M). (For interpretation of the references to color in this figure legend, the reader is referred to the web version of this article.)

interaction pathways can be considered in **II**. The Ce···Ce distances across the Ce···OCO···Ce and Ce···SO<sub>4</sub>···Ce bridges are 5.2637(8) and 6.5583(18) Å, respectively, suggesting that the observed anti-ferromagnetic interaction should arise from the magnetic super exchange through these two types of bridges [45,46].

#### 4. Conclusion

We have successfully synthesized {[Ce<sub>2</sub>(PDA)<sub>3</sub>(H<sub>2</sub>O)<sub>3</sub>]·H<sub>2</sub>O<sub>0.25</sub>]<sub>n</sub> (**I**) and {[Ce<sub>2</sub>(PDA)<sub>2</sub>(H<sub>2</sub>O)<sub>5</sub>SO<sub>4</sub>]·2H<sub>2</sub>O]<sub>n</sub> (**II**) by a hydrothermal method. 3D structures of complex **I** and 3D structures of complex **II** are formed through π–π interactions and hydrogen bonds. Both **I** and **II** are stable at high temperature. The magnetic study of **II** confirms that it presents antiferromagnetic behavior. The luminescent properties of complex **I** showed selectivity toward Cu<sup>2+</sup>, Zn<sup>2+</sup>, Cd<sup>2+</sup> and Mn<sup>2+</sup> ions and the luminescent properties of complex **II** showed selectivity toward Pb<sup>2+</sup> ions. Therefore, both complexes may be considered as selective luminescent probe for these metals.

#### Acknowledgments

This work was supported by the Natural Science Foundation of Henan Province, P.R. China (No. 13A150056, 12B150005, 122102210174 and 12B150004).

#### Appendix A. Supplementary material

CCDC 860241 and 848801 contain the supplementary crystallographic data for this paper. This data can be obtained free of charge from The Cambridge Crystallographic Data Centre via <http://www.ccdc.cam.ac>.

#### References

- [1] Yang L-R, Song S, Shao C-y, Zhang W, Zhang H-M, Bu Z-W, et al. Synthesis, structure and luminescent properties of two-dimensional lanthanum(III) porous coordination polymer based on pyridine-2,6-dicarboxylic acid. *Synthetic Metals* 2011;161(11–12):925–30.
- [2] Eddaoudi M. Systematic design of pore size and functionality in isorecticular MOFs and their application in methane storage. *Science* 2002;295(5554):469–72.
- [3] Seo JS, Whang D, Lee H, Im Jun S, Oh J, Jeon YJ, et al. A homochiral metal–organic porous material for enantioselective separation and catalysis. *Nature* 2000;404(6781):982–6.
- [4] Shi F, Cunha-Silva L, Ferreira RAS, Mafra L, Trindade T, Carlos L, et al. Interconvertible modular framework and layered lanthanide (III)–etidronic acid coordination polymers. *Journal of the American Chemical Society* 2008;130(1):150–67.
- [5] Robin AY, Fromm KM. Coordination polymer networks with O- and N-donors: what they are, why and how they are made. *Coordination Chemistry Reviews* 2006;250(15–16):2127–57.
- [6] Ouyang Y, Zhang W, Xu N, Xu GF, Liao DZ, Yoshimura K, et al. Three-dimensional 3d–4f polymers containing heterometallic rings: syntheses, structures, and magnetic properties. *Inorganic Chemistry* 2007;46(21):8454–6.
- [7] Hu M, Wang QL, Xu GF, Zhao B, Deng GR, Zhang YH, et al. Synthesis and characterization of a novel lanthanide coordination polymer with network structure based on [Er<sub>4</sub>([mu] 3-OH) 4]8+ cluster and 2, 2'-bipyridine-3, 3'-dicarboxylate. *Inorganic Chemistry Communications* 2007;10(10):1177–80.
- [8] Zhao B, Yi L, Dai Y, Chen XY, Cheng P, Liao DZ, et al. Systematic investigation of the hydrothermal syntheses of Pr(III)-PDA (PDA = pyridine-2, 6-dicarboxylate anion) metal–organic frameworks. *Inorganic Chemistry* 2005;44(4):911–20.
- [9] Ghosh SK, Bharadwaj PK. Self-assembly of lanthanide helicate coordination polymers into 3D metal–organic framework structures. *Inorganic Chemistry* 2004;43(7):2293–8.
- [10] Hou H, Wei Y, Song Y, Fan Y, Zhu Y. First octameric ellipsoid lanthanide (III) complexes: crystal structure and nonlinear optical absorptive and refractive properties. *Inorganic Chemistry* 2004;43(4):1323–7.
- [11] Gao HL, Yi L, Zhao B, Zhao XQ, Cheng P, Liao DZ, et al. Synthesis and characterization of metal–organic frameworks based on 4-hydroxypyridine-2, 6-dicarboxylic acid and pyridine-2, 6-dicarboxylic acid ligands. *Inorganic Chemistry* 2006;45(15):5980–8.
- [12] Zhu T, Ikarashi K, Ishigaki T, Uematsu K, Toda K, Okawa H, et al. Structure and luminescence of sodium and lanthanide(III) coordination polymers with pyridine-2,6-dicarboxylic acid. *Inorganica Chimica Acta* 2009;362(10):3407–14.
- [13] Zhao B, Cheng P, Dai Y, Cheng C, Liao DZ, Yan SP, et al. A Nanotubular 3D coordination polymer based on a 3d–4f heterometallic assembly. *Angewandte Chemie International Edition* 2003;42(8):934–6.
- [14] Wu JY, Yeh TT, Wen YS, Twu J, Lu KL. Unusual robust luminescent porous frameworks self-assembled from lanthanide ions and 2, 2'-bipyridine-4, 4'-dicarboxylate. *Crystal Growth & Design* 2006;6(2):467–73.
- [15] Prasad T, Rajasekharan M. A novel water octamer in Ce (dipic) 2 (H<sub>2</sub>O) 3 ⊙ 4H<sub>2</sub>O: crystallographic, thermal, and theoretical studies. *Crystal Growth & Design* 2006;6(2):488–91.
- [16] Zhao B, Chen XY, Cheng P, Liao DZ, Yan SP, Jiang ZH. Coordination polymers containing 1D channels as selective luminescent probes. *Journal of the American Chemical Society* 2004;126(47):15394–5.
- [17] Tanase S, Gallego PM, de Gelder R, Fu WT. Synthesis, crystal structure and photophysical properties of europium (III) and terbium (III) complexes with pyridine-2, 6-dicarboxamide. *Inorganica Chimica Acta* 2007;360(1):102–8.
- [18] Brouca-Cabarrecq C, Dexpert-Ghys J, Fernandes A, Jaud J, Trombe JC. Synthesis, crystal structures and properties of three new lanthanide 2, 6-pyridinedicarboxylate complexes with zero-dimensional structure. *Inorganica Chimica Acta* 2008;361(9):2909–17.
- [19] Mahata P, Ramya K, Natarajan S. Synthesis, structure and optical properties of rare-earth benzene carboxylates. *Dalton Transactions* 2007;(36):4017–26.
- [20] Kurmoo M. Magnetic metal–organic frameworks. *Chemical Society Reviews* 2009;38(5):1353–79.
- [21] Yang S, Lin X, Blake AJ, Thomas KM, Hubberstey P, Champness NR, et al. Enhancement of H<sub>2</sub> adsorption in Li+-exchanged co-ordination framework materials. *Chem Communications* 2008;(46):6108–10.
- [22] Dong YB, Wang P, Ma JP, Zhao XX, Wang HY, Tang B, et al. Coordination-driven nanosized lanthanide “Molecular Lantern” with tunable luminescent properties. *Journal of the American Chemical Society* 2007;129(16):4872–3.
- [23] Morris RE, Wheatley PS. Gas storage in nanoporous materials. *Angewandte Chemie International Edition* 2008;47(27):4966–81.
- [24] Halim M, Tremblay MS, Jockusch S, Turro NJ, Sames D. Transposing molecular fluorescent switches into the near-IR: development of luminogenic reporter substrates for redox metabolism. *Journal of the American Chemical Society* 2007;129(25):7704–5.
- [25] Davis ME. Ordered porous materials for emerging applications. *Nature* 2002;417(6891):813–21.
- [26] Lee JY, Farha OK, Roberts J, Scheidt KA, Nguyen SBT, Hupp JT. Metal–organic framework materials as catalysts. *Chemical Society Reviews* 2009;38(5):1450–9.
- [27] Feng ML, Kong DN, Xie ZL, Huang XY. Three-dimensional chiral microporous germanium antimony sulfide with ion-exchange properties. *Angewandte Chemie International Edition* 2008;120(45):8751–4.
- [28] Allendorf M, Bauer C, Bhakta R, Houk R. Luminescent metal–organic frameworks. *Chemical Society Reviews* 2009;38(5):1330–52.
- [29] Wang P, Ma JP, Dong YB, Huang RQ. Tunable luminescent lanthanide coordination polymers based on reversible solid-state ion-exchange monitored by ion-dependent photoinduced emission spectra. *Journal of the American Chemical Society* 2007;129(35):10620–1.
- [30] Li JR, Kuppler RJ, Zhou HC. Selective gas adsorption and separation in metal–organic frameworks. *Chemical Society Reviews* 2009;38(5):1477–504.
- [31] Nucci NV, Scott JN, Vanderkooi JM. Coupling of complex aromatic ring vibrations to solvent through hydrogen bonds: effect of varied on-ring and off-ring hydrogen-bonding substitutions. *The Journal of Physical Chemistry B* 2008;112(13):4022–35.
- [32] Custelcean R, Gorbunova MG. A metal–organic framework functionalized with free carboxylic acid sites and its selective binding of a Cl (H<sub>2</sub>O) 4-cluster. *Journal of the American Chemical Society* 2005;127(47):16362–3.
- [33] Wang Z, Cohen SM. Postsynthetic modification of metal–organic frameworks. *Chemical Society Reviews* 2009;38(5):1315–29.
- [34] Liu MS, Yu QQ, Cai YP, Su CY, Lin XM, Zhou XX, et al. One-, two-, and three-dimensional lanthanide complexes constructed from pyridine-2, 6-dicarboxylic acid and oxalic acid ligands. *Crystal Growth and Design* 2008;8(11):4083–91.
- [35] Leonard JP, Jensen P, McCabe T, O'Brien JE, Peacock RD, Kruger PE, et al. Self-assembly of chiral luminescent lanthanide coordination bundles. *Journal of the American Chemical Society* 2007;129(36):10986–7.
- [36] Cai M, Chen J, Taha M. Synthesis, structures and antibacterial activities of two complexes of yttrium (III) with 2,6-pyridinedicarboxylate. *Inorganic Chemistry Communications* 2010;13(1):199–202.
- [37] dos Santos CMG, Harte AJ, Quinn SJ, Gunnlaugsson T. Recent developments in the field of supramolecular lanthanide luminescent sensors and self-assemblies. *Coordination Chemistry Reviews* 2008;252(23–24):2512–27.
- [38] Tang R-R, Gu G-L, Zhao Q. Synthesis of Eu(III) and Tb(III) complexes with novel pyridine dicarboxamide derivatives and their luminescence properties. *Spectrochimica Acta Part A: Molecular and Biomolecular Spectroscopy* 2008;71(2):371–6.
- [39] Gregory JK. The water dipole moment in water clusters. *Science* 1997;275(5301):814–7.
- [40] Tancrez N, Feuvrier C, Ledoux I, Zyss J, Toupet L, Le Bozec H, et al. Lanthanide complexes for second order nonlinear optics: evidence for the direct

- contribution of f electrons to the quadratic hyperpolarizability 1. *Journal of the American Chemical Society* 2005;127(39):13474–5.
- [41] Brouca-Cabarrecq C, Trombe JC. Synthesis and crystal structure of three new metal-organic frameworks in the Ln(III)/2,6-pyridinedicarboxylate system. *Journal of Chemical Crystallography* 2009;39(11):786–98.
- [42] Cai Y-P, Yu Q-Y, Zhou Z-Y, Hu Z-J, Fang H-C, Wang N, et al. Metal-directed assembly of two 2-D 4d–4f coordination polymers based on elliptical triple-deck cylinders hinged by meso-double helical chains. *CrystEngComm* 2009;11(6):1006.
- [43] Bo Q-B, Sun Z-X, Forsling W. A new family of 3D 3d–4f heterometallic frameworks comprising 1D inorganic lanthanide ladders and organic Cu-bipyridine chains. *CrystEngComm* 2008;10(2):232.
- [44] Hu Z, Wang Y, Shi D, Tan H, Li X, Wang L, et al. Highly-efficiency red-emitting platinum (II) complexes containing 4'-diarylamino-1-phenylisoquinoline ligands in polymer light-emitting diodes: synthesis, structure, photoelectron and electroluminescence. *Dyes and Pigments* 2010;86(2):166–73.
- [45] Xiao DR, Wang EB, An HY, Li YG, Su ZM, Sun CY. A bridge between pillared-layer and helical structures: a series of three-dimensional pillared coordination polymers with multiform helical chains. *Chemistry-A European Journal* 2006;12(25):6528–41.
- [46] Brouca-Cabarrecq C, Fernandes A, Jaud J, Costes J. Hydrothermal investigation of the lanthanide (Ln = La, Ce, Pr, Nd, Sm) 2, 6-pyridinedicarboxylate system. *Inorganica Chimica Acta* 2002;332(1):54–60.